P2.12 Two-layer patterns of enhanced ZDR in clouds

Jelena Andric[(1)], Dusan Zrnic[(2)], and Valery Melnikov[(3)]

(1) National Severe Storm Laboratory/CIMMS
(2) National Severe Storm Laboratory, Norman, Oklahoma
(3) Cooperative Institute for Mesoscale Meteorological Studies, University of Oklahoma, Norman, Oklahoma

Introduction

Short centimeter and mm-wavelength radars are well suited for remote observation of clouds. These wavelengths provide good detectability of cloud particles with low reflectivity. Kollias et al. (2007) recently published a review of ground-based cloud radars and their applications. Continuously running MM-wavelength Cloud Radars (MMCR), operated by the Atmospheric Radiation Measurement (ARM) program, have vertically pointed beams so they obtain cloud parameters above the radars. Matrosov et al. (1996, 2001) and Reinking et al. (2002) obtained the shapes of cloud particles using depolarization measurements at 3-cm wavelength.

5- and 10-cm wavelength radars are used to measure precipitation. Development of precipitation cannot be understood without studying cloud processes. Thus, dual-polarization precipitation radars are becoming a choice instrument for cloud measurements. The NWS is planning to upgrade the WSR-88D network with polarimetric capabilities in the near future (e.g., Istok, et al. 2009). The deployment is scheduled to begin in 2010. The NOAA's research and development polarimetric radar KOUN (a proof of concept for WSR-88D) employs a polarimetric mode with simultaneous transmission and reception of horizontally (H) and vertically (V) polarized waves (Zrnic et al., 2006).

In addition to the standard spectral moments, the KOUN routinely measures the following polarimetric variables: 1) differential reflectivity, 2) the differential phase, and 3) copolar correlation coefficient (e.g., Doviak and Zrnic, 2006, section 6.8). Signals from clouds are often weak, and thus noise influence on polarimetric variables can be strong. To mitigate noise impact at low SNR, the covariance estimators of polarimetric variables are used on the time series data from the KOUN (Melnikov and Zrnic, 2007). Differential reflectivity and the correlation coefficient fields in clouds exhibit patterns with "pockets" and layers of high and low values demonstrating the complexity of cloud processes.

Ikeda et al. (2004) studied stratiform clouds with two layers of enhanced differential reflectivity produced by the presence of two melting layers at different heights. Matrosov et al. (2006) analyzed situations in which the upper layer was in the region of

Corresponding author address: J. Andric, University of Oklahoma, Norman, OK 73072; jelena.andric@noaa.gov

subfreezing temperature and thus could not have been caused by melting.

Two-layers of enhanced differential reflectivity are considered in this paper. The upper layer is situated at heights where the temperature was subfreezing. We consider growth processes of cloud particles that can form enhanced differential reflectivity aloft in such conditions. Radar data from KOUN and C-band dual-polarization radar of the Environment of Canada are analyzed.

1. Background

a) Polarimetric variables

WSR-88D KOUN radar employs a polarimetric mode with simultaneous transmittion and reception of horizontally and vertically polarized waves. The amplitudes of the transmitted and received waves will be denoted by E_h, E_v and E_{hr}, E_{vr}. Transmittion of polarized radio-waves, their scattering by particles, and reception of the scattered waves can be described by the following matrix equation (e.g., Doviak and Zrnic, 2006, 8.5.2.1):

$$\begin{pmatrix} E_{hr} \\ E_{vr} \end{pmatrix} = \begin{pmatrix} S_{hh} & S_{hv} \\ S_{hv} & S_{vv} \end{pmatrix} \begin{pmatrix} E_h \\ E_v \end{pmatrix},$$

where S_{ij} are the scattering matrix coefficients of the medium. Range dependence and radar constants in this equation are omitted without loss of generality because we are interested in polarimetric parameters that do not depend on those. Powers P_h and P_v in the receive channels and the correlation function R_{hv} between received waves are:

$$P_h = <| E_{hr} |^2>, \qquad P_v = <| E_{vr} |^2>,$$
$$R_{hv} = < E_{hr}^* E_{vr} >,$$

where the brackets stand for ensemble averaging and the asterisk denotes complex conjugate. Radar reflectivity factor Z_h is strongly dependent on particle size and concentration; it is defined as:

$$Z_h = 10\log\left[\frac{P_h - N_h}{N_h}\right] + 20\log(R) + C_r$$

where N_h is noise power in the horizontal channel, R is distance to radar volume, and C_r is the radar constant. Differential reflectivity Z_{DR} and copolar correlation coefficient ρ_{hv} are defined by

$$Z_{DR} = 10\log\frac{P_h - N_h}{P_v - N_v},$$
$$\rho_{hv} = \frac{| R_{hv} |}{[(P_h - N_h)(P_v - N_v)]^{1/2}}$$

The reflectivity factor (Z_h) is proportional to the cross section of a hydrometeor and is weighted heavily by hydrometeors of largest diameter within the volume. Z_{DR} is independent of concentration but depends on shape, alignment, size, density and phase composition of the particles. Z_{DR} values in ice clouds are determined by ratios of major and minor axis of crystals, their densities and their orientations. ρ_{hv} is sensitive to the diversity of particle sizes, orientations, shapes and irregularities, and the phase compositions within the radar sampling volume.

b) Ice growth process

The occurrence of ice crystals in clouds is related to cloud type, temperature, saturation and stage of cloud development. The growth of ice particles is described by 3 growth process: deposition - growth of ice particles by diffusion of water vapor; accretion or riming - growth by collision with supercooled droplets that subsequently freeze, and aggregation - collision with other crystals that produces clusters of ice crystals, called aggregates. Water-saturated cloud that has high supersaturation with respect to ice represents favorable conditions for depositional growth. These conditions will last as long as water droplets are available to evaporate and maintain the vapor pressure at equilibrium relative to water, Rodgers and Yau 1989.

Crystal habit is a function of temperature and supersaturation with respect to ice. Figure 1 shows a new habit diagram that presents such dependence, adopted from Bailey and Hallett, 2008. This diagram is obtained from laboratory results and pictures from cloud particle imager (CPI). Unlike Magono and Lee 1966, new diagram emphasizes that most ice crystals are defective and irregular in shape and are mostly polycrystalline at temperatures below -20ºC. Also, the diagram shows different habits for temperatures below -20ºC, compared to Magono and Lee habit diagram. The traditional diagrams agree with the new one for temperatures at approximately -18ºC. Plate-like growth regime is between approximately -20ºC and -40ºC, and columnar regime is from -40ºC to -70 ºC, according to the new diagram.

Red rectangle in Fig. 1, indicates crystal habits that are of interest in this study; these include plate-like crystals and different types of dendrites.

Based on the observations done by Korolev et al, 2000, maximum frequency of occurrence of dendrites was observed in the temperature interval -15 ºC < T < -10 ºC, which is consistent with laboratory results and natural conditions (e.g. Hallett and Mason 1958, Magono and Lee 1966). However, there are cases where (in this temperature range) instead of dendrites dominant crystal habit is irregular. Also, Korolev (2000) found that dendritic ice particles occur in isolated cells embedded in zones of irregular shaped ice particles that can reach fraction of 100% in those cells. A particle starts to exhibit dendritic features when it reaches some 400 – 600 μm in size. Mason (1994) provided computations for final diameter of ice crystals that had fallen from -20ºC temperature level to 0ºC in water saturated environment. He assumed that crystal retains the same habit during fall. He concluded that stellar dendrites can reach final size of 5.3 mm.

In certain temperature range in a cloud, and for certain shape and size of a crystal, growth by aggregation becomes dominant. It is a process of collision and coalescence that produce clusters of ice crystals. Highest probability of snowflakes occurrence is on levels with temperature close to 0ºC. Probability decreases with decreasing temperature and it reaches secondary maximum at -15ºC. Aggregates of dendritic crystals tend to become large and typical diameter is between 2 and 5 mm. Aggregates have low density and they are more spherical in shape compare with pristine plate crystals. Formation of aggregates will cause increase in Z_h and decrease in Z_{DR} value. This process is

dominant at lower temperatures (-15ºC) and high ice crystal concentrations.

c) Calculations of Z_{DR}

A simple scattering consideration assumes change of density and aspect ratio along with reflectivity factor and differential reflectivity for dendrites and aggregates. In order to specifically account for these crystal habits, we used the relationships between density and diameter of crystals, Pruppacher and Klett 1980.
For density of dendrites, a power low dependence on diameter is:

$$\rho_{den} = 0.588 D^{-0.377},$$

and for density of aggregates it is

$$\rho_{agg} = 0.178 D^{-0.922}.$$

The aspect ratio for dendrites is calculated from the power low relation

$$h = \alpha L^{\beta},$$

where *h* denotes minor and *L* major axis of the crystal. Values for α and β are taken from Matrosov et al. (1996). Because aggregates are mostly irregular in shape, there is no power low that gives relationship between minor and major axes of aggregate. Given the observed low values of Z_{DR} in regions of aggregates, it is expected that these hydrometeors would have roughly spherical shape, so their spect ratio would be close to one. Because of the complexity of their shape we used two constant values for the aspect ratio 0.3 and 0.8, Matrosov et al. 1996. In his study, Matrosov modeled aggregates as both prolate and oblate spheroids to account for their shape complexity. Also, Korolev (2000) has found that roundness is a function of particle size, and not temperature. Aspect ratio, on the other hand, of particles within the range of 60 μm to 1000 μm, is mainly function of temperature and not size of the particle. For temperature range from 0ºC to -20ºC, the aspect ratio is about 0.6 with very small deviations about this mean value.
Z_{DR} is computed from

$$Z_{DR} = 10 \log \left(\frac{\int_0^{D_{\max}} |f_h|^2 N(D) dD}{\int_0^{D_{\max}} |f_v|^2 N(D) dD} \right),$$

where f_h and f_v are scattering amplitudes defined as:

$$f_{v,h} = \frac{D^3}{L_{a,b} + \frac{1}{\varepsilon - 1}} C,$$

where $L_{a,b}$ is the shape parameter, ε is the dielectric constant and C is a constant that does not effect Z_{DR}.
The following exponential distribution

$$N(D) = N_o \exp(-\Lambda D)$$

is used. Here, N_o is the intercept parameter and Λ is the slope parameter.
Low density of this crystal habits effects dielectric constant which is smaller compared to dielectric constant of solid ice. Thus, dielectric constant is calculated as a function of density for both dendrites and aggregates**.**
Also, we assume that the slope parameter is changing approximately from 1 mm^{-1} to 6 mm^{-1}. This choice is based on computations done by

Passarelli (1978) for average spectra at the four different altitudes (the exact values are 24.4, 38.5 55.0 65.0 cm^{-1}). In the early stage of growth process, concentration of small particles is higher, and with their growth size distribution gets wider. This will produce decrease of slope parameter with increasing diameter.

2. Observations

a) Synoptic situation

Upper level trough, with intense jet stream (over 120 knots) crossing over Oklahoma, provided favorable dynamical conditions for convective-type mixed winter precipitation. A cold front has passed Oklahoma the previous day, so this was a post frontal situation with the cloud system moving from NW toward SE.
Base reflectivity from KTLX radar of a cloud cover spreading over SE, S, E and NE of Oklahoma along with location of KTLX radar is given in Figure 2. This PPI is made at the same time as RHI by KOUN radar (located 20 km from KTLX). Black line signifies azimuthal direction of 181°. Enhanced values of reflectivity factor (35 to 40 dBZ) indicate locations where mixed-type precipitation occurred.

Because the radar data was obtained near midnight, a morning sounding from OUN 28 January 2009 at 00 UTC is used for temperature and saturation profile, Fig. 3. Cloud top was at approximately 7.3 km, and temperature at that level was -26°C. There were two frizzing levels very close to each other (upper one is at ~2.2 km, lover at ~1.4 km). Subfreezing temperatures in the lowest partition of troposphere (below 1.4 km) and a layer of warmer air (with temperature slightly above 0ºC) above and below freezing level caused mixed precipitation in form of sleet, and freezing rain in some areas.
Throughout the whole cloud, relative humidity with respect to water ranged from 80% to 100%. Saturation with respect to ice is less than saturation with respect to water. Thus, atmosphere was supersaturated with respect to ice at all levels where saturation over water reached 100%.

b) Observed polarimetric data

Radar data were collected at azimuth 181° and are presented as vertical cross-sections, RHI (Range Height Indicator). Only a snap shot (no time evolution) of RHI was made on 27 January 2009 at 2317 UTC. Vertical cross-sections of Z_h and Z_{DR} are given in Fig. 4. Enhanced values of Z_h (around 45 dBZ) show location of a melting layer between 40 km and ~80 km. Reflectivity factor alone doesn't provide much information regarding microphysical structure of this cloud. However, in the lower panel of Fig. 4, one can notice "pockets" of high Z_{DR} (nearly 3 dB) that coincide with lower value of Z_h (about 20 DBZ). These indicate ice crystal growth and changes of their growth habit. Our focus will be on the radar signature above the melting layer (>2 km) and on an explanation of enhanced Z_{DR} signature in terms of processes that may have lead to these signatures. We hypothesize that Z_{DR} increase is related to horizontal growth, mainly by deposition, of dendrites and relatively fast transition to growth by aggregation. At the beginning of aggregation few crystals clump together to make a larger, well oriented, and relatively dense aggregate. As a result Z_{DR} signature is pronounced at

approximately 5 km. As aggregates grow their density is decreasing, which produces lower Z_{DR} and ρ_{hv} regardless of their shape and orientation. Aggregation leads to a wider size distribution of snowflakes, which causes lower ρ_{hv}.

Another example of enhanced Z_{DR} signature, in subfreezing temperature area, is evident in radar polarimetric data measured by a C band radar near Toronto in Canada. Figure 5 represents composite RHI of Z_h, Z_{DR} and ρ_{hv} in azimuthal direction of 310°, measured on December 23, 2004 in the Toronto area. Both Z_{DR} and ρ_{hv} have signatures between 3.5 and 4.5 km which are very similar to the melting layer, but are not related to melting. According to soundings, temperature in this layer was between -5°C and -10° C. Strong vertical gradient of Z_h indicates rapid aggregation of snow crystals. At ranges closer to radar, up to 30 – 35 km, vertical gradient of Z_h is smaller and Z_{DR} and ρ_{hv} signatures are less pronounced, indicating that aggregation at higher levels is weaker.

3. Nature of enhanced Z_{DR} signatures at subfreezing temperatures

Vertical profiles of Z_h, ρ_{hv} and Z_{DR} shown in Fig. 6 are made through the layer of enhanced Z_{DR} (fig. 4) at the distance of 45 km from the radar. We will consider four characteristic layers between five levels as shown in Fig. 6. Levels are marked as H_o for the ground, H_1 for the upper bound of melting layer, H_2 for enhanced Z_{DR} signature aloft, H_3 for beginning of Z_{DR} enhancements, and H_4 for the cloud top. Layer 1 is between H_4 and H_3, layer 2 is between H_3 and H_2, layer 3 is between H_2 and H_1, and the last layer includes the bright band and precipitation. On the right axis, temperatures from sounding are given.

Layer 1: starting from H_4, Z_h gradually increases and Z_{DR} remains small and almost constant. Within this layer crystals grow by deposition of water vapor; this is the first stage of ice crystals growth. Deposition is a very slow process and crystals remain nearly spherical in shape. Z_{DR} values are slightly above zero until they reach level H_3. Dielectric constant in layer 1 is ε = 3.15, which corresponds to solid ice. Plate-like crystal habit is expected at this temperature range and small supersaturation over ice.

Layer 2: In this layer, Z_h continues to increase due to crystals' growth. Expected crystal habit at this temperature range (from -10°C to -16°C) is dendritic (Bailey and Hallett 2008, Korolev 2000). Z_{DR} starts increasing after reaching H_3 level. The reason for this is that crystals have reached certain threshold for thickness and they continued to grow only in horizontal direction. Depositional growth of dendrites dominates in this layer.

Layer 3: Z_{DR} reaches maximum of 2.5 dB at H_2, and after that begins to decrease rapidly. We speculate that aggregation starts at this level. As aggregates grow, they become more spherical in shape and their density decreases. Thus, Z_{DR} decreases to nearly zero. Z_h is sill increasing due to large size of aggregates (in this layer, reflectivities exceed 30 dBZ). At H_2, temperature is approximately -10°C, which is favorable for significant aggregation (Rodgers 1989). Rapid Z_{DR} increase is followed by decrease in ρ_{hv} values (minimum of 0.95 is at H_2). This trend continues to level H_1.

Layer 4: At the top of the layer, melting of aggregates occurs because

they reach zero temperature. In this paper we focus on cloud processes that take place in layers 1, 2, and 3.

Based on the ice crystal habit diagram (Figure 1), and in situ measurements (Korolev et al. 2000), we assume that enhanced Z_{DR} signature is produced by dendrites within layer 2 (Fig. 6). Rapid decrease of Z_{DR} below that layer is related to formation of aggregates.

Figure 7 shows change of density of dendrites (blue line) and aggregates (red line) with increasing diameter. The density of dendrites that have diameter smaller than 200 μm, is equal to the density of solid ice. Once the diameter of particle reaches 200 μm, the density starts decreasing to a minimum of 0.2 g cm^{-1} at particle's size of bout 5 mm. The density of aggregates decreases more rapidly. This decrease of density strongly affects the dielectric constant and decreases Z_{DR}.

In Figure 8, calculated Z_{DR} for individual dendrites (panel a) and for a range of diameters (panel b) are presented for different slope parameter Λ of the DSD. Maximum Z_{DR} (panel a) corresponds to the transition point from dendrites to aggregates with sizes of about 200 μm. The aspect ratios begins to decrease at sizes of 60 μm (not shown), but density decrease contributes significantly to the Z_{DR} drop. Also, the panel 8b shows that for larger dendrites (small slope parameter), Z_{DR} is below 0.2 dB. For small dendrites, which correspond to larger slope parameter, Z_{DR} is below 3 dB.

For aggregates, no analytical relationship between the aspect ratio and diameter is available. Thus, three different values of the aspect ratio, i.e., 0.3, 0.6, and 0.8, are used to produce individual Z_{DR} and Z_{DR} averaged over range of diameters in Figure 9. Aggregates have lower Z_{DR} compared to dendrites for all three values of aspect ratios. Z_{DR} is below 0.8 dB for all three cases. It is seen also that aspect ratio does not influence averaged Z_{DR} as much as individual ones. Also, as in the case with dendrites, the effect of decreasing density dominates.

4. Conclusion

Observation of vertical profiles of polarimetric variables through non precipitation clouds have been made by the KOUN polarimetric radar in Norman OK. Clear signatures in differential reflectivity and reflectivity suggest growth of aligned crystals in the upper tier of the cloud followed by aggregation and then melting at the zero degree isotherm. These observations are consistent with conceptual explanations based on computed profiles of the involved polarimetric variables. In future studies a microphysical model will be combined with the scattering computations to solidify and quantify these preliminary conclusions.

Acknowledgments: The authors thank to Dr. Alexander Ryzhkov and Dr. Pamela Heinselman for their helpful comments and suggestions.

References

Doviak, R. J. and D. S. Zrnic, 2006: Doppler radar and weather observations, 2nd ed., Dover Publications, 562 pp.

Ikeda, K., E.A. Brandes, and R.M. Rasmussen, 2005: Polarimetric Radar Observation of Multiple Freezing Levels. *J. Atmos. Sci.*, **62**, 3624–3636.

Istok, M., M. Fresch, Z. Jing, S. Smith, R. Murnan, A. Ryzhkov, J. Krause, M. Jain, P. Schlatter, J. Ferree, B. Klein, D. Stein, G. Cate, R. Saffle, 2009: WSR-88D dual-polarization initial operational capabilities. *25*th *Conf. on IIPS, Amer. Meteorol. Soc*., Phoenix, AZ, 15.6.

Korolev, A.V., G.A. Isaac and J. Hallett, 2000: Ice particle habits in stratiform clouds. *Quart.J.R. Met. Soc.*, **126**, 2873-2902.

Korolev, A., and G. Isaac, 2003: Roundness and Aspect Ratio of Particles in Ice Clouds. *J. Atmos. Sci.*, **60**, 1795–1808.

Magono, C. and C.W. Lee, 1966: Meteorological classification of natural snow crystals. *Jour.Fac. Sci., Hokkaido* Univ. Series VII, **2**, 321-335.

Matrosov, S.Y., R.F. Reinking, R.A. Kropfli, and B.W. Bartram, 1996: Estimation of Ice Hydrometeor Types and Shapes from Radar Polarization Measurements. *J. Atmos. Oceanic Technol.*, **13**, 85–96.

Matrosov, S. Y., R.F. Reinking, R.A. Kropfli, B. E. Martner, and B.W. Bartram, 2001: On the use of radar depolarization ratios for estimating shapes of ice hydrometeors in winter clouds. *J. Applied Meteorol.*, **40**, 479-490.

Melnikov, V.M., and D.S. Zrnić, 2007: Autocorrelation and Cross-Correlation Estimators of Polarimetric Variables. *J. Atmos. Oceanic Technol.*, **24**, 1337–1350.

Pruppacher, H. R. and J. D. Klett, 1980: *Microphysics of Clouds and Precipitation*. D. Reidel, 508pp.

Passarelli, R.E., 1978: Theoretical and Observational Study of Snow-Size Spectra and Snowflake Aggregation Efficiencies. *J. Atmos. Sci.*, **35**, 882–889.

Reinking, R. F., S. Y. Matrosov, R. A. Kropfli, and B.W. Bartram, 2002: Evaluation of a 45-slant quasi-linear radar polarization state for distinguishing drizzle droplets, pristine ice crystals, and less regular ice particles. *J. Atmos. Oceanic Technol.*, **19**, 296-321.

Rogers, R.R. and M.K. Yau., 1989: *A Short Course in Cloud Physics*, 3rd. ed. Elsevier Press, 160 pp

Ryzhkov, A. V., Pinsky A., Khain A., 2009: Polarimetric radar observation operator for a cloud model with spectral microphysics. Submitted to the *J.Atmos. Sci.*

Zrnic D.S., V. M. Melnikov, and J. K. Carter, 2006: Calibrating differential reflectivity on the WSR-88D. *J. Atmos. Ocean. Technol*., **23**, 944-951.

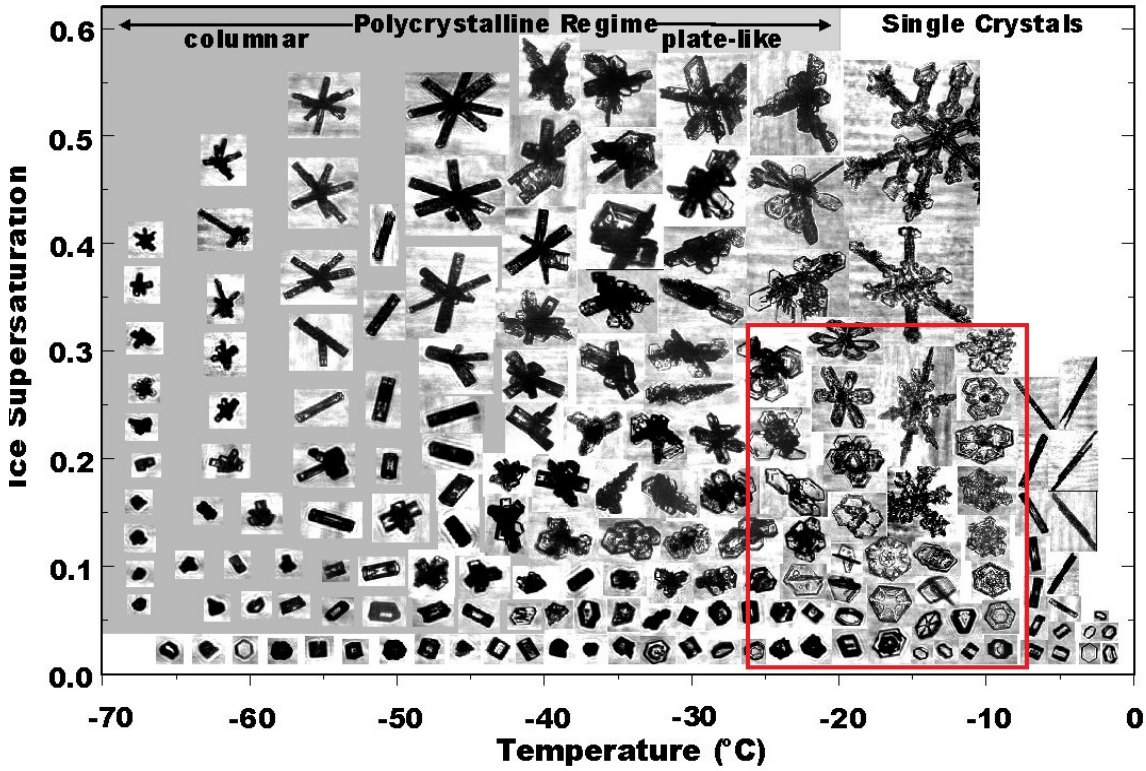

Figure 1. Habit diagram in pictorial format for atmospheric ice crystals derived from laboratory results and CPI; red rectangle signifies ice crystal habits that belong to temperature and ice supersaturation range of interest for our case; from Bailey and Hallett, 2008.

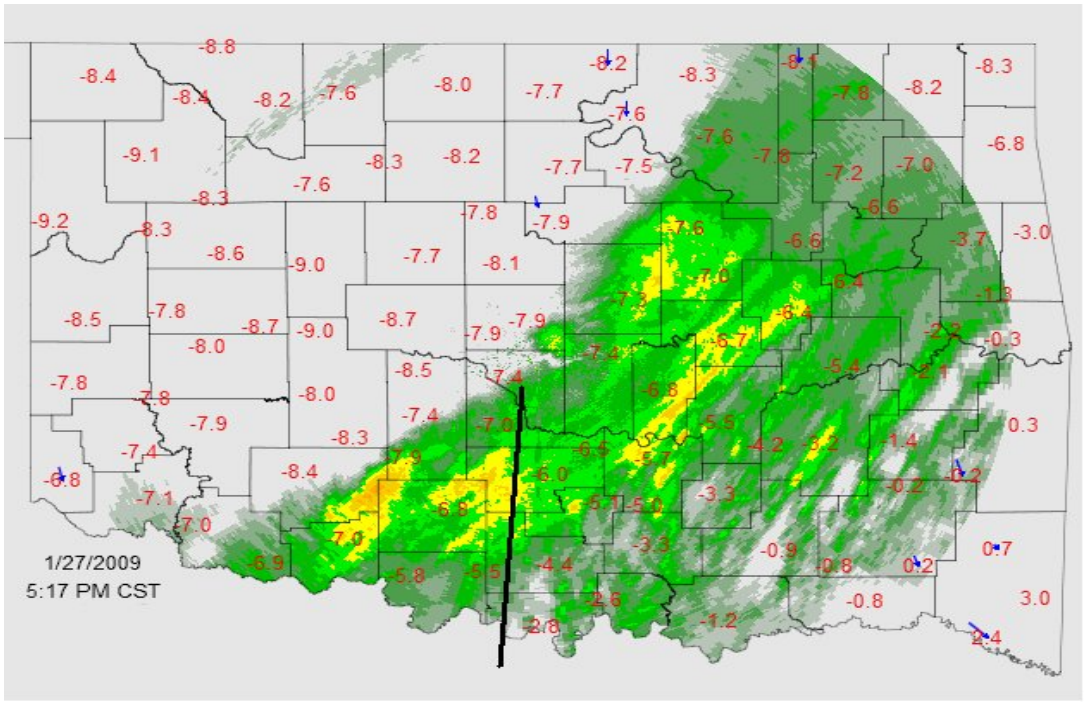

Figure 2. PPI at the time the RHI is made; the black line denotes the direction of RHI (azimuth angle of 181°) with respect to the KTLX radar*; red numbers are surface temperatures (from the Oklahoma Mesonet).*

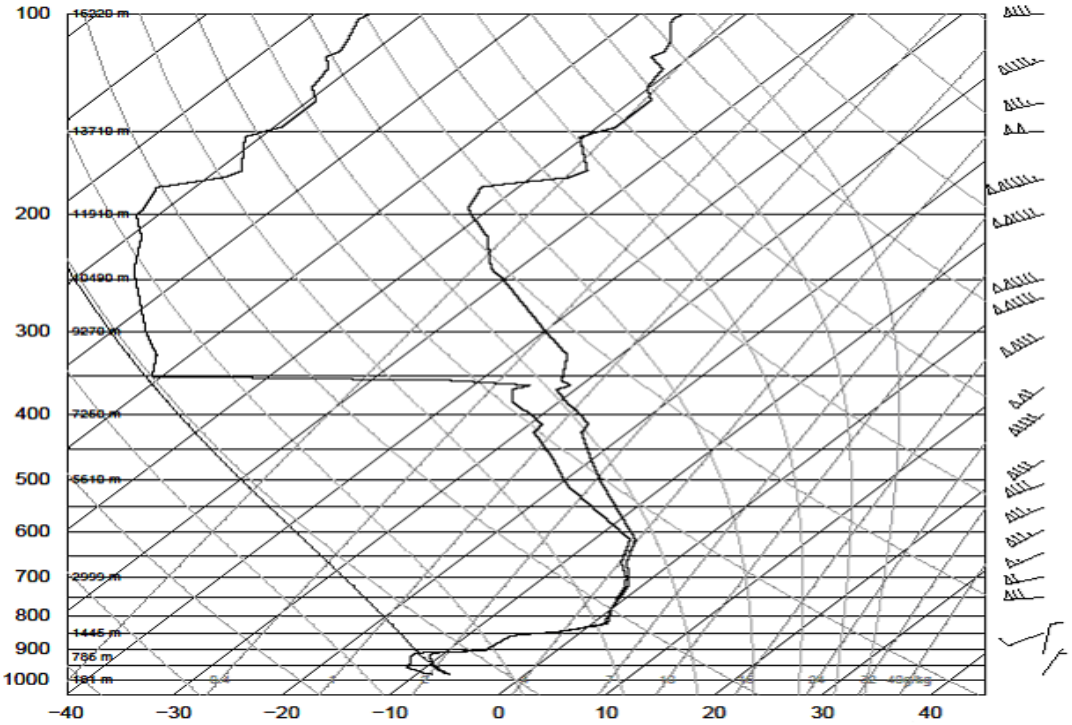

Figure 3. Sounding, at OUN 28 January 2009, 00Z.

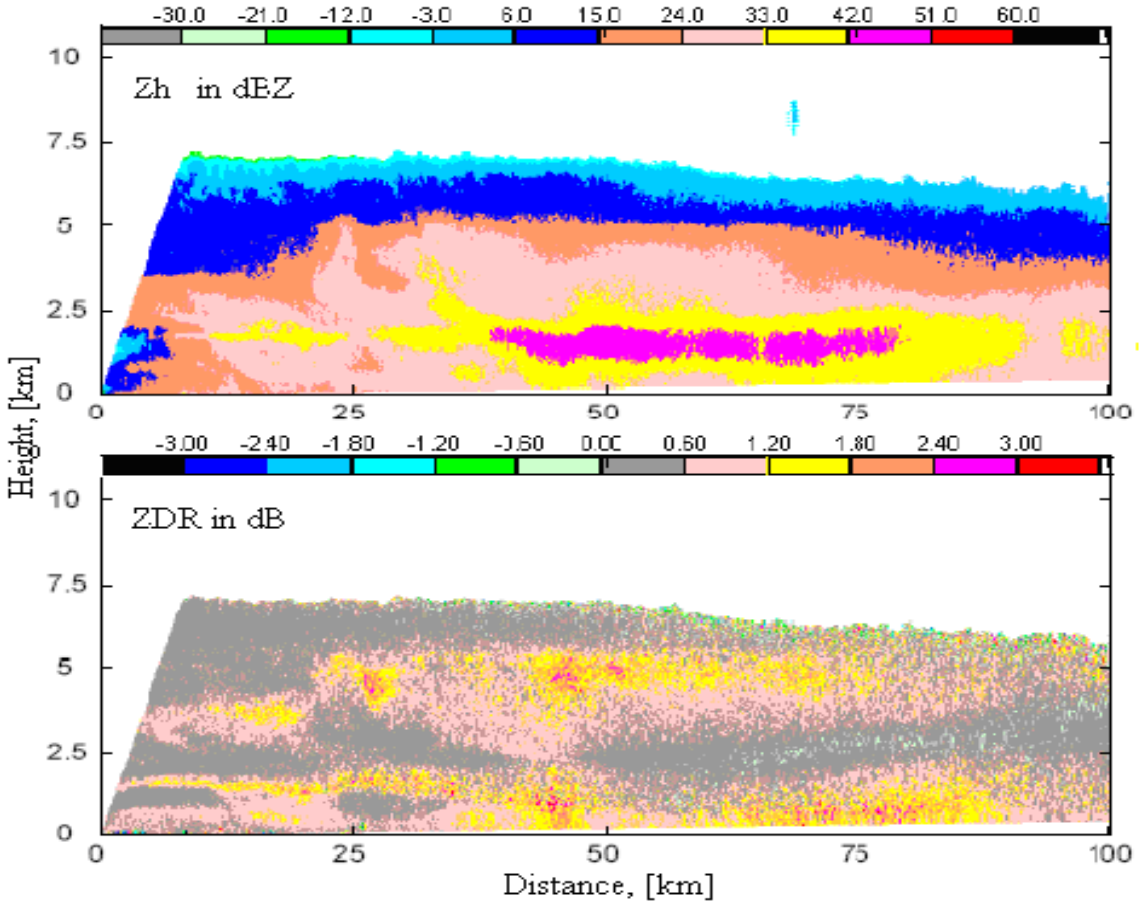

Figure 4. RHI of Z_{DR} and Z_h at the azimuth of 181° measured by KOUN radar on January 27, 2009.

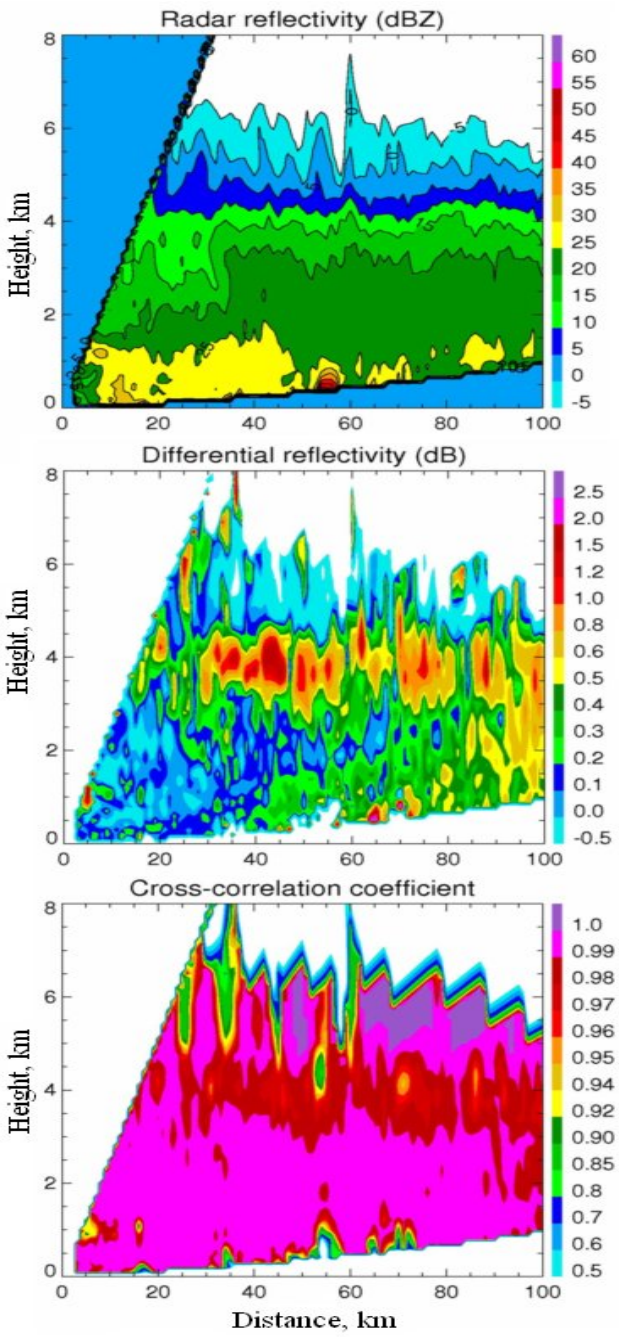

Figure 5. Composite RHI of Z_h, Z_{DR} and ρ_{hv} at 310° azimuth, measured by the C band radar on December 23, 2004; High Z_{DR} and ρ_{hv} are within the layer between 3.5 and 4.5 km.

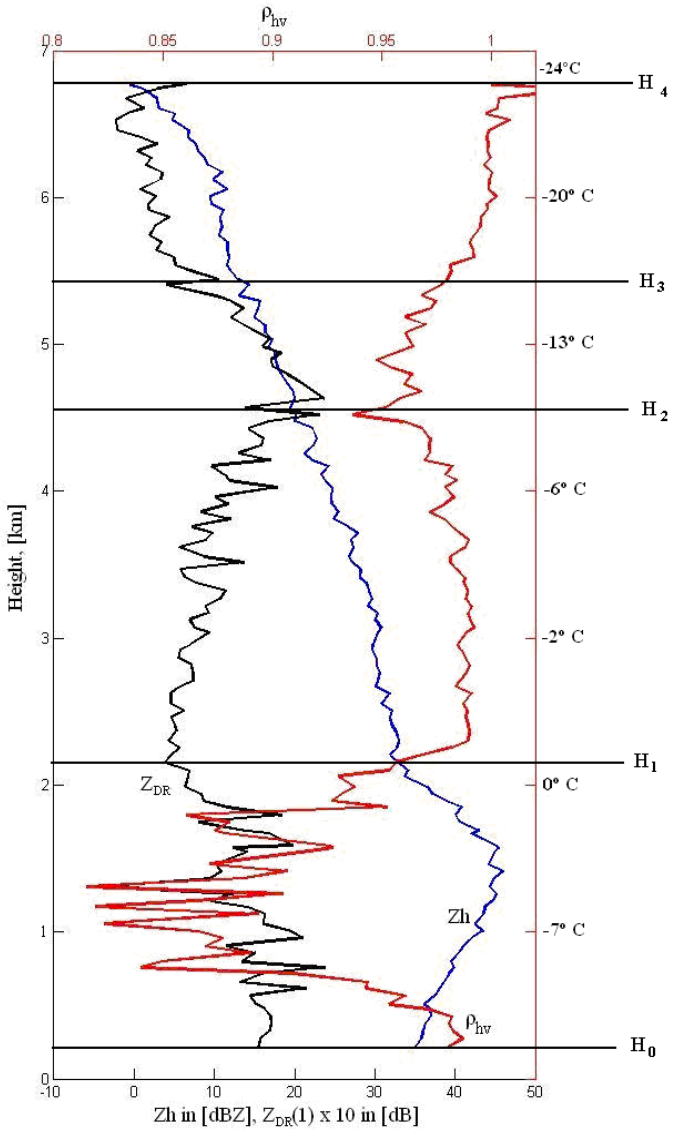

Figure 6. *Vertical profile of reflectivity factor (Z_h), differential reflectivity Z_{DR} and ρ_{hv}, at 45 km from the radar; on the right axis is the temperature from soundings at indicated levels.*

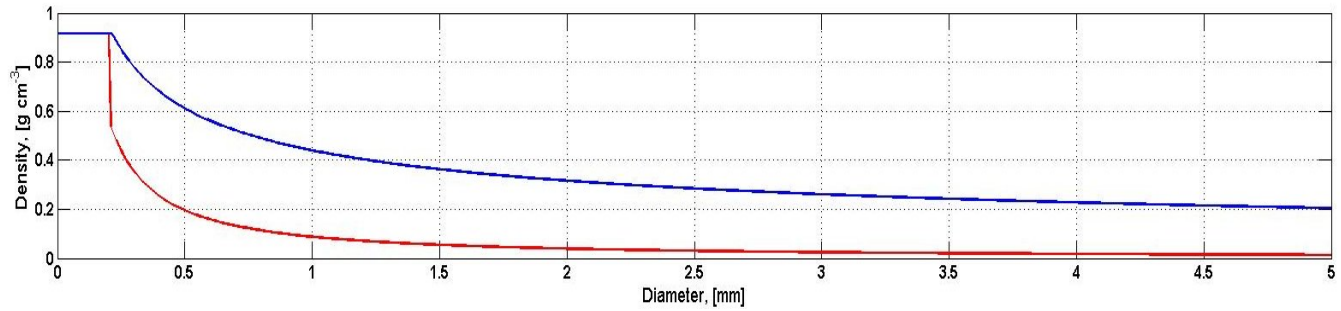

Figure 7. The density of dendrites (blue line) and aggregates (red line), as a function of diameter.

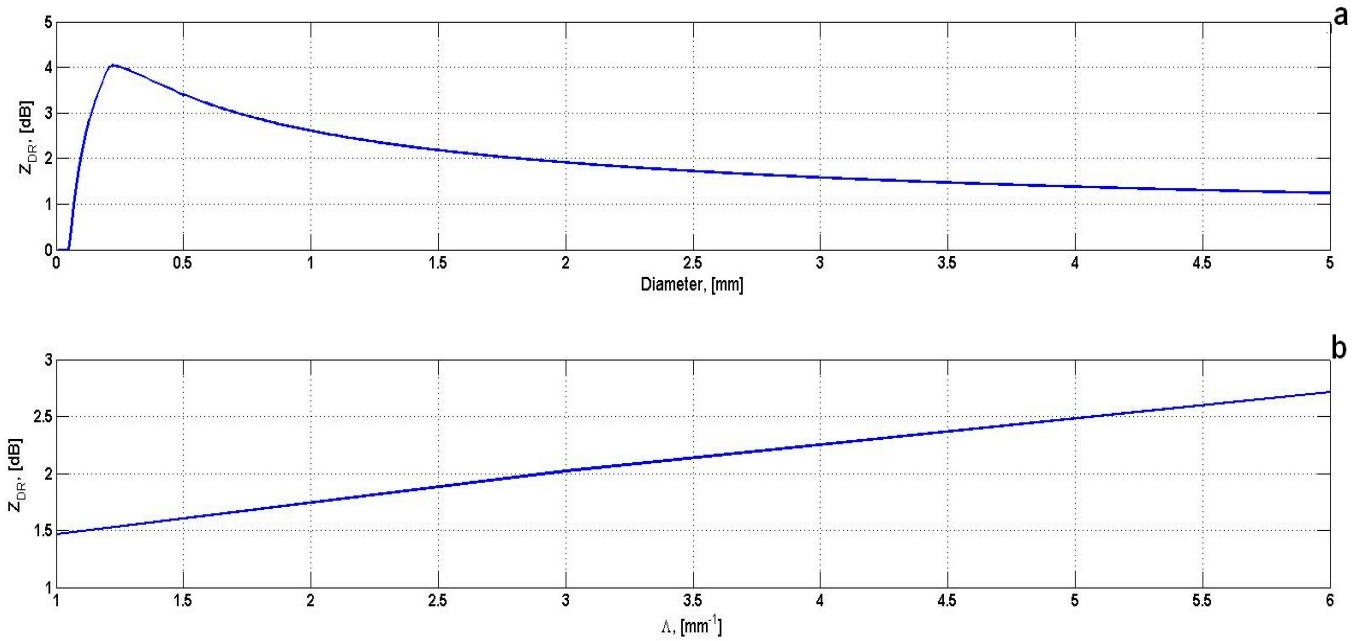

Figure 8. (a) Z_{DR} calculated for individual particles of dendrites as a function of diameter; (b) Z_{DR}, calculated from the distribution of sized as a function of slope parameter.

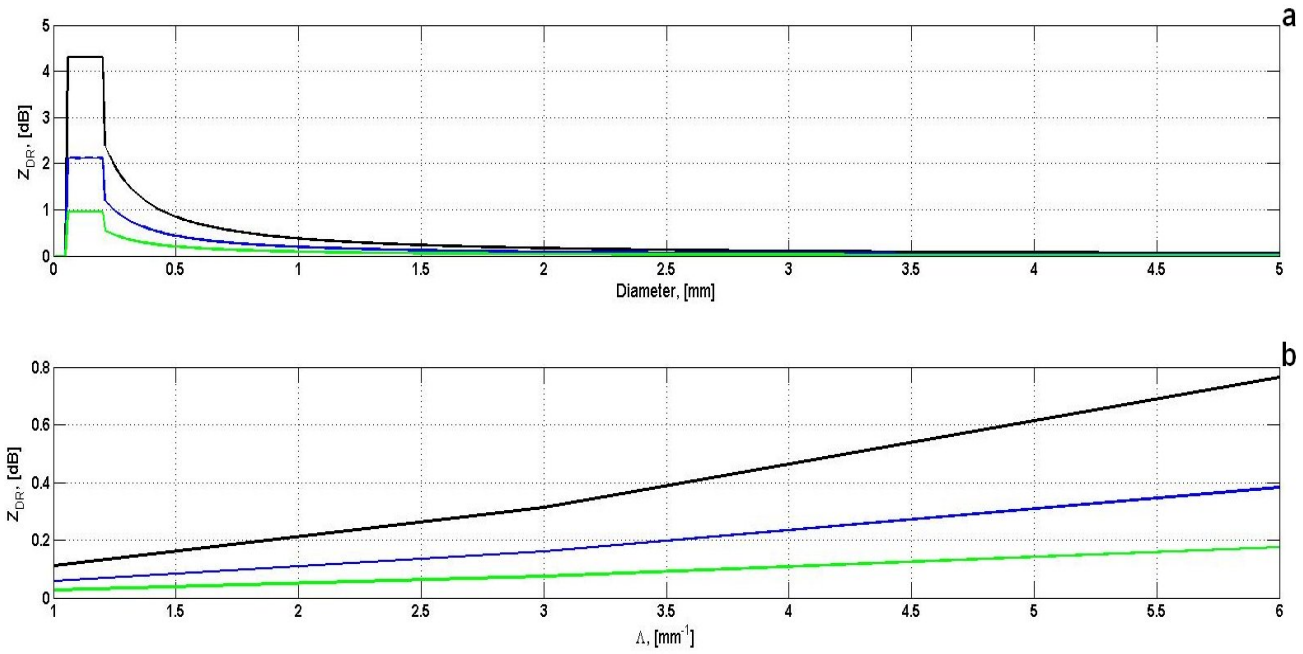

Figure 9. (a) Z_{DR} calculated for individual particles of aggregates as a function of diameter and for different values of aspect ratio, the green line denotes the aspect ratio 0.8, the blue line is for 0.6, and the black lines is for 0.3; (b) Z_{DR}, calculated for a range of diameters as a function of slope parameter for r=0.8 (green line), r=0.6 (blue line) and r=0.3 (black line).